Thermodynamics and Finite size scaling in Scalar Field Theory

A thesis submitted to the

Tata Institute of Fundamental Research, Mumbai

for the degree of

Master of Science, in Physics

By

Debasish Banerjee

Department of Theoretical Physics, School of Natural Sciences

Tata Institute of Fundamental Research, Mumbai

December 2008

Synopsis

In this work we study the thermodynamics of an interacting ϕ^4 theory in 4 space-time dimensions. The expressions for the thermodynamic quantities are worked out, anisotropic lattice regularization is explained. The renormalisation conditions are discussed and expression for the β and the γ functions are obtained in perturbation theory to 1 loop order. The anisotropy coefficients are also calculated to 1 loop order in perturbation theory. This is the first report for the calculation of the anisotropy coefficient in an interacting ϕ^4 theory. The algorithms used for a non-perturbative study and their numerical implementation are discussed. The results obtained using these algorithms are compared with the existing results in the literature. The choice of the points on which the simulations were done is justified. The procedure of removing the ultraviolet divergence via subtraction is described. Finally, the use of finite size scalings to establish the thermodynamic limit for the obtained results is elaborated upon.

Acknowledgements

I would like to thank Sourendu Gupta for suggesting this problem and both Sourendu Gupta and Saumen Datta for patiently guiding me through the maze of numerical computations and stressing the relevant physics issues involved. I am quite indebted to Rajiv Gavai for the knowledge of Lattice Field Theory I acquired in the course that he gave on the topic. With great pleasure, I acknowledge all the physics discussions that I have had with my friends and colleagues including Arnab, Sayantan, Loganayagam, Jyotirmoy, Swastik, Shamayita and Shamik in this regard. Without the unfailing support from my parents through all my education, this thesis would not have been possible.

Contents

List of Tables

List of Figures

Chapter 1

Introduction

Scalar field theories are simple and pedagogically important for the study of many important concepts in quantum field theory. Besides, they have been seriously considered to shed light on real physics issues, such as in the Higgs sector of the Standard Model. Techniques involving resummation of Feynman diagrams to control the infra-red singularity that arise in bosonic field theories at finite temperatures have been first applied to the case of the scalar ϕ^4 theory before trying to use them to obtain thermodynamics of quantum chromodynamics.

In this thesis, we aim to study the equation of state non-perturbatively on the lattice for the case of the 1-component real ϕ^4 theory in the symmetric phase. At zero temperature, this model has been extensively studied to establish its triviality in the continuum limit [1] [2] [3] [4]. Finite size investigations of physical quantities have been studied in [5] [6] [7]. Algorithmic improvements have also been tested on this model in [8] [9]. Thermodynamics of lattice theories were first studied in the context of gauge fields [10] [11] [12]. For scalar fields the first studies were naturally on free systems and involved a systematic study of the cut-off effects [13] [14]. Issues of zero mode contributions for massless scalar theories were studied in [15] [16]. Finite temperature studies of a lattice ϕ^4 theory using variational approximation were treated in [17] [18].

Chapter 2

Setting up the thermodynamics

Consider a theory with Hamiltonian H at a physical temperature $\beta = 1/T$. The partition function is given by

$$\mathcal{Z}(\beta) = Tr(e^{-\beta H}) \tag{1}$$

The thermal expectation value of an operator $\mathcal{O}$ (that depends on the fields φ) in path integral notation is

$$\langle \mathcal{O}(\varphi) \rangle = \frac{1}{\mathcal{Z}(\beta)} \int \mathcal{D}\varphi e^{-\beta H} \mathcal{O}(\varphi) \tag{2}$$

For a finite temperature study, the extents in the spatial directions, $L_1 = L_2 = L_3 = L$, must be much larger than the extent in the temporal direction, T; i.e, $L \gg T$. In addition the bosonic fields must satisfy periodic boundary conditions while the fermionic ones are imposed with anti-periodic boundary conditions.

2.1 Lattice Thermodynamics

The thermodynamic quantities of interest are obtained as derivatives of the partition function $\mathcal{Z}$. If $V = L^3 = (N_s a)^3$ denotes the spatial volume and $T = \beta^{-1} = (N_t a)^{-1}$ the temperature, where a is the lattice spacing and N_s and N_t are the

number of lattice points in the spatial and temporal directions respectively, then the expressions for the energy density and pressure are

$$E = -\frac{1}{V}\frac{\partial \ln \mathcal{Z}}{\partial \beta}\bigg|_V = \frac{T^2}{V}\frac{\partial \ln \mathcal{Z}}{\partial T}\bigg|_V \tag{3}$$

$$P = T\frac{\partial \ln \mathcal{Z}}{\partial V}\bigg|_T \tag{4}$$

Note that these formulae require taking derivatives with respect to the "temperature" keeping the "volume" constant. To facilitate this procedure, the system is formulated on an anisotropic lattice with the spacing along the time and space directions taken to be a_t and a_s respectively. The anisotropy parameter is defined as:

$$\xi = \frac{a_s}{a_t} \tag{5}$$

In our analysis, we use a_t to scale all dimensional quantities since it is the one most naturally linked to temperature. The set (a_t,ξ) will be chosen as the set of independent parameters and all expressions involving a_s will be re-expressed as a function of these two quantities.

Now, for example, to get E the volume is to be kept constant while taking derivative with respect to the temperature. This amounts to differentiating with respect to a_t holding a_s constant. In this formalism this is implemented by using a change of variables to re-express this derivative as:

$$\frac{\partial}{\partial a_t}\bigg|_{a_s} = -\frac{\xi}{a_t}\frac{\partial}{\partial \xi}\bigg|_{a_t} + \frac{\partial}{\partial a_t}\bigg|_{\xi} \tag{6}$$

After substituting for V and T, the expressions for the quantities of interest are

$$Ea_t^4 = \frac{1}{N_s^3 N_t}\frac{1}{\xi^3}\left\{\xi\frac{\partial \ln \mathcal{Z}}{\partial \xi}\bigg|_{a_t} - a_t\frac{\partial \ln \mathcal{Z}}{\partial a_t}\bigg|_{\xi}\right\} \tag{7}$$

$$Pa_t^4 = \frac{1}{3N_s^3 N_t}\frac{1}{\xi^2}\frac{\partial \ln \mathcal{Z}}{\partial \xi}\bigg|_{a_t} \tag{8}$$

$$(E-3P)a_t^4 = -\frac{1}{N_s^3 N_t}\frac{a_t}{\xi^3}\frac{\partial \ln \mathcal{Z}}{\partial a_t}\bigg|_{\xi} \tag{9}$$

Note that the quantities Ea_t^4, Pa_t^4 and $(E-3P)a_t^4$ are all dimensionless quantities and will henceforth be referred to as E, P and $E-3P$ respectively in lattice

units. The derivatives of the couplings of the theory with respect to the anisotropy parameter ξ are known as the anisotropy coefficients. This work reports the first evaluation of the anisotropy coefficients for the scalar ϕ^4 theory, the details of which are discussed in section 2.2.3.

2.2 The lattice ϕ^4 theory

The action of the scalar field theory in continuum Euclidean space:

$$S[\phi] = \int dt \int d^3x \left\{ \frac{1}{2}\partial_\mu\phi(x)\partial_\mu\phi(x) + \frac{1}{2}m_0^2\phi(x)^2 + \frac{g_0}{4!}\phi(x)^4 \right\} \tag{10}$$

where m_0 is the bare mass and g_0 is the bare self-coupling.
The action on the lattice is obtained by replacing the derivatives ∂_μ by finite differences Δ_i defined as

$$\Delta_i f(x) = \frac{f(x+a_i) - f(x)}{a_i} \tag{11}$$

where a_i is the lattice spacing along the direction i. To go to the standard form of the action for doing simulations we trade off the set of couplings (g_0, m_0) in favour of (κ, λ). They are related to each other by the following implicit set of equations:

$$\kappa = \frac{1-2\lambda}{3\xi + \xi^3 + ((a_t m_0)^2/2)\xi^3}; \quad \kappa_t = \kappa_s\xi^2 = \kappa\xi^3; \quad \lambda = \frac{g_0}{24}\xi^3\kappa^2 \tag{12}$$

Further, scaling out the dimensions of the mass and the field

$$\hat{\phi} = a_t\frac{\phi}{\sqrt{\kappa}}; \quad \hat{m}_0 = a_t m_0 \tag{13}$$

the action can be recast in the form of a generalized spin model

$$\begin{aligned} S[\hat{\phi}] \;=\; & \sum_{x_\alpha} \left\{ -\kappa_s \sum_{i=1}^{3} \hat{\phi}(x_\alpha + a_i)\hat{\phi}(x_\alpha) - \kappa_t\hat{\phi}(x_\alpha + a_t)\hat{\phi}(x_\alpha) \right. \\ & \left. + \hat{\phi}(x_\alpha)^2 + \lambda(\hat{\phi}(x_\alpha)^2 - 1)^2 \right\} \end{aligned} \tag{14}$$

This is the conventional form for doing simulations. Henceforth all the hatted quantities are dimensionless.

While studying the thermodynamics, it is useful to measure the thermodynamic quantities as relative shifts from their zero temperature values, which also serve to cancel the zero temperature divergent terms in the corresponding quantities. Thus we renormalise the pressure to be zero at $T = 0$, or in other words we measure $P(T) - P(0)$. This is true for the energy density and $E - 3P$ as well. To achieve this the expectation value of the operators calculated in the zero temperature limit are subtracted from their finite temperature counterparts. This procedure will be denoted by adding the subscript "subt" to the operators. In terms of the action S the expression of the thermodynamic quantities become:

$$\begin{aligned} Ea_t^4 &= \frac{1}{\xi^3}\left\{-\xi\left\langle \left.\frac{\partial S}{\partial \xi}\right|_{a_t}\right\rangle_{subt} + \left\langle \left. a_t\frac{\partial S}{\partial a_t}\right|_{\xi}\right\rangle_{subt}\right\} \\ Pa_t^4 &= -\frac{1}{3\xi^2}\left\langle \left.\frac{\partial S}{\partial \xi}\right|_{a_t}\right\rangle_{subt} \\ (E-3P)a_t^4 &= \frac{1}{\xi^3}\left\langle \left. a_t\frac{\partial S}{\partial a_t}\right|_{\xi}\right\rangle_{subt} \end{aligned} \tag{15}$$

where bracketed quantities denote expectation values taken with respect to the probability density $\rho[\phi] = e^{-S[\hat{\phi}]}/\mathcal{Z}$. Thus in order to proceed we need to find explicit expressions for the anisotropy coefficients (derivatives of the couplings with respect to ξ) and the β- and γ- functions (derivatives of the couplings with respect to a_t). This evaluation will be attempted in 1-loop perturbation theory. The rationale for using perturbation theory at this level will be discussed in a later chapter. After calculating the expressions for the physical quantities, ξ is set to unity.

2.2.1 Renormalization conditions

This sub-section just sets the conventions used in this work. These are mainly adopted from [21] which the reader can consult for details. The anisotropic propagator is

$$G(k) = \langle \hat{\phi}(k)\hat{\phi}(-k)\rangle = \frac{1}{\kappa}\frac{1}{4\xi\sum_{i=1}^{3}\sin^2(k_i/2) + 4\xi^3\sin^2(k_4/2) + \xi^3\hat{m}_0^2} \tag{16}$$

In 1 loop perturbation theory the Feynman diagrams that need to be summed to get the renormalized quantities are shown in fig(1). The square of the renormalized mass is defined to be the negative of the two-point renormalized vertex function at zero external momentum:

$$\hat{m}_R^2 = -\Gamma_R^{(2)}(0) \tag{17}$$

On the other hand, the physical mass ma, measured from the correlators is defined to be the poles of the propagator at zero external momentum and is related to $\hat{m}_R$ through the relation:

$$\hat{m}_R = 2\sinh\left(\frac{ma}{2}\right) \tag{18}$$

The renormalized coupling is defined through the four-point vertex function at zero external momentum:

$$g_R = -\Gamma_R^{(4)}(0,0,0,0) \tag{19}$$

2.2.2 Evaluation of the β and γ functions

Equation (15) requires the evaluation of the following derivatives:

$$\begin{aligned} d_{\kappa_s} &= a_t\frac{\partial\kappa_s}{\partial a_t}\bigg|_\xi ; \; d_{\kappa_t} = a_t\frac{\partial\kappa_t}{\partial a_t}\bigg|_\xi ; \; d_\lambda = a_t\frac{\partial\lambda}{\partial a_t}\bigg|_\xi \\ c_{\kappa_s} &= \kappa_s'|_{a_t} ; \qquad c_{\kappa_t} = \kappa_t'|_{a_t} ; \qquad c_\lambda = \lambda'|_{a_t} \end{aligned}$$

where

$$f' = \frac{\partial f(\xi)}{\partial\xi} \tag{20}$$

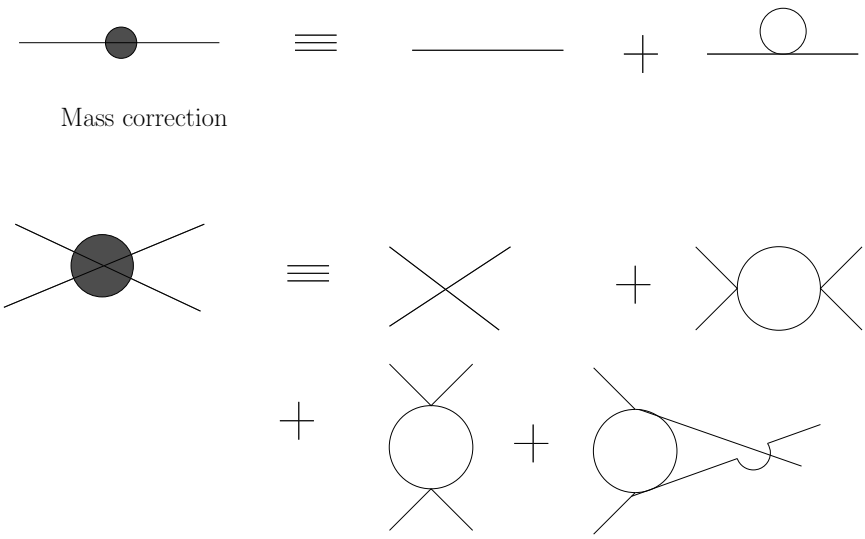

Figure 1: The Feynman diagrams that need to be calculated

The first three of these derivatives are completely specified by the β- and γ- functions defined as

$$\begin{aligned} \beta(g_0) &= a_t \left.\frac{\partial g_0}{\partial a_t}\right|_\xi \\ \gamma(\hat{m_0}) &= a_t \left.\frac{\partial \hat{m_0}^2}{\partial a_t}\right|_\xi \end{aligned} \tag{21}$$

The evaluation of these two functions is standard and is discussed in detail in [21]. Here, we simply write down the final formulae upto 1 loop order noting that while taking this derivative with respect to a_t one needs to keeps ξ constant.

$$\begin{aligned} a_t \left.\frac{\partial \hat{m}_0^2}{\partial a_t}\right|_\xi &= a_t \left.\frac{\partial \hat{m}_R^2}{\partial a_t}\right|_\xi \left[1 - \frac{g_R}{2}\left(\frac{1}{16\pi^2}\ln(\hat{m}_R^2) + \frac{1}{16\pi^2} + r_1\right)\right] \\ a_t \left.\frac{\partial g_0}{\partial a_t}\right|_\xi &= \frac{3}{2} g_R^2 \, a_t \left.\frac{\partial J_2(\hat{m}_R, \xi)}{\partial a_t}\right|_\xi \\ J_2(m_R, \xi) &= \int_0^\infty dx \; x e^{-x(\xi^3 m_R^2 + 6\xi + 2\xi^3)} I_0^3(2\xi x) I_0(2\xi^3 x) \end{aligned} \tag{22}$$

where r_1 is a constant and $I_n(x)$ denotes the modified Bessel function of order n. In perturbation theory, we have:

$$\begin{aligned} a_t \frac{\partial \hat{m}_R^2}{\partial a_t}\bigg|_{\xi=1} &= 4ma \sinh(\frac{ma}{2}) \cosh(\frac{ma}{2}) \\ a_t \frac{\partial J_2(\hat{m}_R^2)}{\partial a_t}\bigg|_{\xi=1} &= -\frac{ma}{16\pi^2} \coth(\frac{ma}{2}) \end{aligned} \tag{23}$$

In the continuum limit (when scaling violations disappear) the first universal coefficient β_0 of the beta-function can be worked out to be $\frac{3}{16\pi^2}$. The other coefficients can be written down using these expressions:

$$\begin{aligned} d_{\kappa_s} = a_t \frac{\partial \kappa_s}{\partial a_t}\bigg|_{\xi=1} &= -\frac{1}{4+\hat{m}_0^2/2+(g_0\kappa)/6} \left[a_t \frac{\partial g_0}{\partial a_t}\bigg|_{\xi=1} \frac{\kappa^2}{12} + \frac{1-2\lambda}{2(4+\hat{m}_0^2/2)}\, a_t \frac{\partial \hat{m}_0^2}{\partial a_t}\bigg|_{\xi=1} \right] \\ d_{\kappa_t} = a_t \frac{\partial \kappa_t}{\partial a_t}\bigg|_{\xi=1} &= a_t \frac{\partial \kappa_s}{\partial a_t}\bigg|_{\xi=1} \\ d_\lambda = a_t \frac{\partial \lambda}{\partial a_t}\bigg|_{\xi=1} &= a_t \frac{\partial g_0}{\partial a_t}\bigg|_{\xi=1} \frac{\kappa^2}{24} + \frac{g_0\kappa}{12}\, a_t \frac{\partial \kappa_s}{\partial a_t}\bigg|_{\xi=1} \end{aligned} \tag{24}$$

2.2.3 Evaluation of the anisotropy coefficients

The anisotropy coefficients that need to be evaluated for the scalar theory are κ_s', κ_t' and λ'. Here they are evaluated to one-loop order only. They can in turn be expressed in terms of $(\hat{m}_0^2)'$ and g_0' appearing in the Lagrangian and can be evaluated from the renormalized vertex functions. To evaluate the mass-squared anisotropy parameter we sum the relevant diagrams in fig. (1) and obtain the following formula:

$$(\hat{m}_0^2)'\big|_{\xi=1} = \frac{g_R}{2} \int_0^\infty x dx e^{-(\hat{m}_R^2+8)x} \left[(3\hat{m}_R^2+12) I_0^4(2x) - 12 I_0^3(2x) I_1(2x) \right] \tag{25}$$

where $I_n(x)$ denotes the modified Bessel function of order n. While differentiating with respect to ξ, a_t is kept constant and since m is already a constant, $\hat{m}_R$ as a whole is constant. Using exactly the same techniques and summing the relevant

diagrams we obtain the anisotropy coefficient for the self coupling:

$$\begin{aligned} g_0'|_{m_R,a_t=const} &= \frac{3}{2} g_R^2 \, J_2'|_{m_R,a_t=const} \\ J_2'|_{m_R,a_t=const} &= \int_0^\infty x^2 dx e^{-x(\hat{m}_R^2+8)} \left[12 I_0^3(2x) I_1(2x) - (3\hat{m}_R^2 + 12) I_0^4(2x) \right] \end{aligned} \tag{26}$$

where g_0 and g_R refer to the bare and renormalized quantities respectively. Using these expressions the anisotropy coefficients for κ_s, κ_t and λ are:

$$\begin{aligned} c_{\kappa_s} = \kappa_s'|_{a_t} &= -\frac{1}{(4 + \hat{m}_0^2/2 + (g_0\kappa)/6)} \left[g_0'|_{a_t} \frac{\kappa^2}{12} + \frac{g_0\kappa^2}{12} + \right. \\ &\qquad \left. + \frac{(1-2\lambda)(2 + \hat{m}_0^2 + \frac{1}{2}\,(\hat{m}_0^2)'|_{a_t})}{4 + \hat{m}_0^2/2} \right] \\ c_{\kappa_t} = \kappa_t'|_{a_t} &= 2\kappa + \kappa_s'|_{a_t} \\ c_\lambda = \lambda'|_{a_t} &= g_0'|_{a_t} \frac{\kappa^2}{24} + \frac{g_0\kappa^2}{24} + \frac{g_0\kappa}{12} \, \kappa_s'|_{a_t} \end{aligned} \tag{27}$$

While calculating these expressions numerically one must be careful about large numbers. Although the numerical values of the coefficients may be small, they involve a rather delicate subtraction among the Bessel functions. The routines given in the Numerical Recipes [22] generate numbers that often exceed the range of the common C compilers. The actual evaluation of these coefficients were therefore done using Mathematica [23] which could handle much larger ranges of the functional values.

2.3 Expressions for thermodynamic quantities

Compact expressions for the thermodynamics observables in dimensionless notation:

$$\begin{aligned} Ea_t^4 &= \left(\langle\sum_{i=1}^{3}\hat{\phi}(x_\alpha+a_i)\hat{\phi}(x_\alpha)\rangle_{sub}\right)\left(c_{\kappa_s}|_{a_t}-d_{\kappa_s}|_{\xi}\right) \\ &+ \left(\langle\hat{\phi}(x_\alpha+a_t)\hat{\phi}(x_\alpha)\rangle_{sub}\right)\left(c_{\kappa_t}|_{a_t}-d_{\kappa_t}|_{\xi}\right) \\ &+ \left(2\langle\hat{\phi}(x_\alpha)^2\rangle_{sub}-\langle\hat{\phi}(x_\alpha)^4\rangle_{sub}\right)\left(c_{\lambda}|_{a_t}-d_{\lambda}|_{\xi}\right) \qquad (28) \\ Pa_t^4 &= \frac{1}{3}\Bigg[\langle\sum_{i=1}^{3}\hat{\phi}(x_\alpha+a_i)\hat{\phi}(x_\alpha)\rangle_{sub}\left(c_{\kappa_s}|_{a_t}\right)+\langle\hat{\phi}(x_\alpha+a_t)\hat{\phi}(x_\alpha)\rangle_{sub}\left(c_{\kappa_t}|_{a_t}\right) \\ &+ \left(2\langle\hat{\phi}(x_\alpha)^2\rangle_{sub}-\langle\hat{\phi}(x_\alpha)^4\rangle_{sub}\right)\left(c_{\lambda}|_{a_t}\right)\Bigg] \qquad (29) \\ (E-3P)a_t^4 &= -\langle\sum_{i=1}^{3}\hat{\phi}(x_\alpha+a_i)\hat{\phi}(x_\alpha)\rangle_{sub}\left(d_{\kappa_s}|_{\xi}\right)-\langle\hat{\phi}(x_\alpha+a_t)\hat{\phi}(x_\alpha)\rangle_{sub}\left(d_{\kappa_t}|_{\xi}\right) \\ &- \left(2\langle\hat{\phi}(x_\alpha)^2\rangle_{sub}-\langle\hat{\phi}(x_\alpha)^4\rangle_{sub}\right)\left(d_{\lambda}|_{\xi}\right) \qquad (30) \end{aligned}$$

Notations

It is to be noted that to maintain uniformity of convention with the figures showing the numerical results, we shall henceforth refer to the operators $\langle\sum_{i=1}^{3}\hat{\phi}(x_\alpha+a_i)\hat{\phi}(x_\alpha)\rangle$ and $\langle\hat{\phi}(x_\alpha+a_t)\hat{\phi}(x_\alpha)\rangle$ as $\langle hops\rangle$ and $\langle hopt\rangle$ respectively. The other operators shall be represented by their usual notations used here.

Chapter 3

Numerical Techniques

The chief tools used in the non-perturbative study of a field theory on the lattice are the Monte-Carlo methods of importance sampling. Using Markov processes, equilibrium configurations are generated such that the probability density for a configuration C is proportional to the Boltzmann factor

$$p_{eq}(C) \propto e^{-S(C)} \tag{31}$$

where $S(C)$ is the action associated with the given configuration. Operators of interest are then measured on these configurations.

3.1 Metropolis Algorithm

Proposed in [19], this algorithm is widely used in numerical simulations. Following pseudo-code describes the method of implementing this algorithm for the case of our interest

1. Choose an initial state

2. Choose a site i

3. Propose a change in the field value at i by a random number generator

4. Calculate the change in the action, ΔS that results from such a change

5. Generate a random number r, s.t. $0 < r < 1$

6. If $r < \exp[-\Delta S]$, then accept the change

7. Go to the next site and repeat from step 3

8. Scanning the entire lattice in this fashion, either site by site or randomly constitutes one sweep.

3.2 Overrelaxation Algorithm

It turns out that the simulations done using local update algorithms, suffer from the defect of critical slowing down. At a critical point, the correlation length of the system diverges due to the dominance of the long distance modes and one needs huge number of local update steps to generate configurations that can be considered to be independent. Overrelaxation algorithms circumvent this problem by making global action preserving changes to make a system move rapidly in the phase space. The overrelaxation algorithm is implemented as follows [9]:

1. Choose a particular site r

2. The local action at that site is

$$S_r = -\kappa\phi(r)h + \lambda[\phi(r)^2 - 1]^2 + \phi(r)^2$$

where $h = \sum_{i=x,y,z,t}[\phi(r+i) + \phi(r-i)]$. At every site, we know the value of ϕ, (say ϕ_0) and hence the action, S_0. This equation can be solved for at least one more real root, ϕ_{new} which will keep the action unchanged.

Table 1: Comparison of the results form Ref. [4] and our work. The parameterset for the runs are ($\lambda = 0.275376, \kappa = 0.288998$). The errors in our work are larger due to smaller runs on smaller lattices.

	$\langle\phi\rangle$	χ_ϕ
Ref.[4]	0.36895 ± 0.00002	12.40 ± 0.05
Our work	0.3689 ± 0.0001	12.34 ± 0.09

3. There is a density of states which needs to be taken into account. For this, calculate $\Delta = \left|\frac{S'[\phi_{new}]}{S'[\phi_{old}]}\right|$, where the bars stand to indicate the absolute value and the differentiation is with respect to ϕ. ϕ_{new} is accepted only if $ran < \Delta$, where ran is a random number between 0 an 1. Morningstar [9] has given a detailed proof that this procedure satisfies detailed balance.

4. Do this on all the lattice sites. This produces a configuration that has the same action; but very different values of ϕ.

The process is deterministic and therefore needs to be coupled to some stochastic local update process in order to generate equilibrium configurations. We do one step of overrelaxation followed by one step of Metropolis and call it one update step.

3.3 Checks of the program

To check the accuracy of our program, simulations were done at ($\lambda = 0.275376, \kappa = 0.288998$) where we measured the vacuum expectation value of the ϕ field and its susceptibility, as defined in eqn (32) and compared it with the results obtained in [4]. The comparisons are displayed in table 1.

$$\chi_\phi = L^4 \left[\langle\phi^2\rangle - \langle|\phi|\rangle^2\right] \tag{32}$$

To get further confidence of the physics results obtained with our program we compared it with the results of the perturbation theory in the vicinity of the critical

point. In this region the physics is expected to be captured by perturbation theory and the agreement would seem natural [2]. In the symmetric phase, we did the simulations at a fixed $\lambda = 0.011153$ for different κ. The mass extracted [20] was compared with the renormalized mass obtained by integrating the Callan-Symanzik equations at constant λ in the vicinity of the critical line where the scaling violations can be neglected. The results shown in fig 2 indicate good agreement. Care was taken to do simulations such that the lattice size exceeded three Compton wavelengths and thus finite size effects small for the respective masses.
Moreover, the perturbation theory result seems to indicate that the phase transition occurs at $\kappa = 0.2544$. This was also checked with our program. The phase transition point was located by looking at the susceptibility curve with the couplings as shown in fig 3. The results perfectly agree with the perturbation theory results.

3.4 Run details of the code

The algorithm that was chosen for the code used to get the physical results was the overrelaxation-Metropolis algorithm. Having verified that our code produces results that are in agreement with the existing values in the literature, the program was optimized to improve the performance.
First, we compared the autocorrelation times in the overrelaxation-Metropolis vs pure Metropolis both near and away from the critical point. The results of this comparison is shown in the fig 4.

The time per spin update and the time required to generate independent configurations in both these algorithms is indicated in table 2. For this comparison, configurations that were separated by $3\tau_{int}$ are taken to be independent. The time measurements for independent configurations was done on a 10^4 lattice at the critical point.

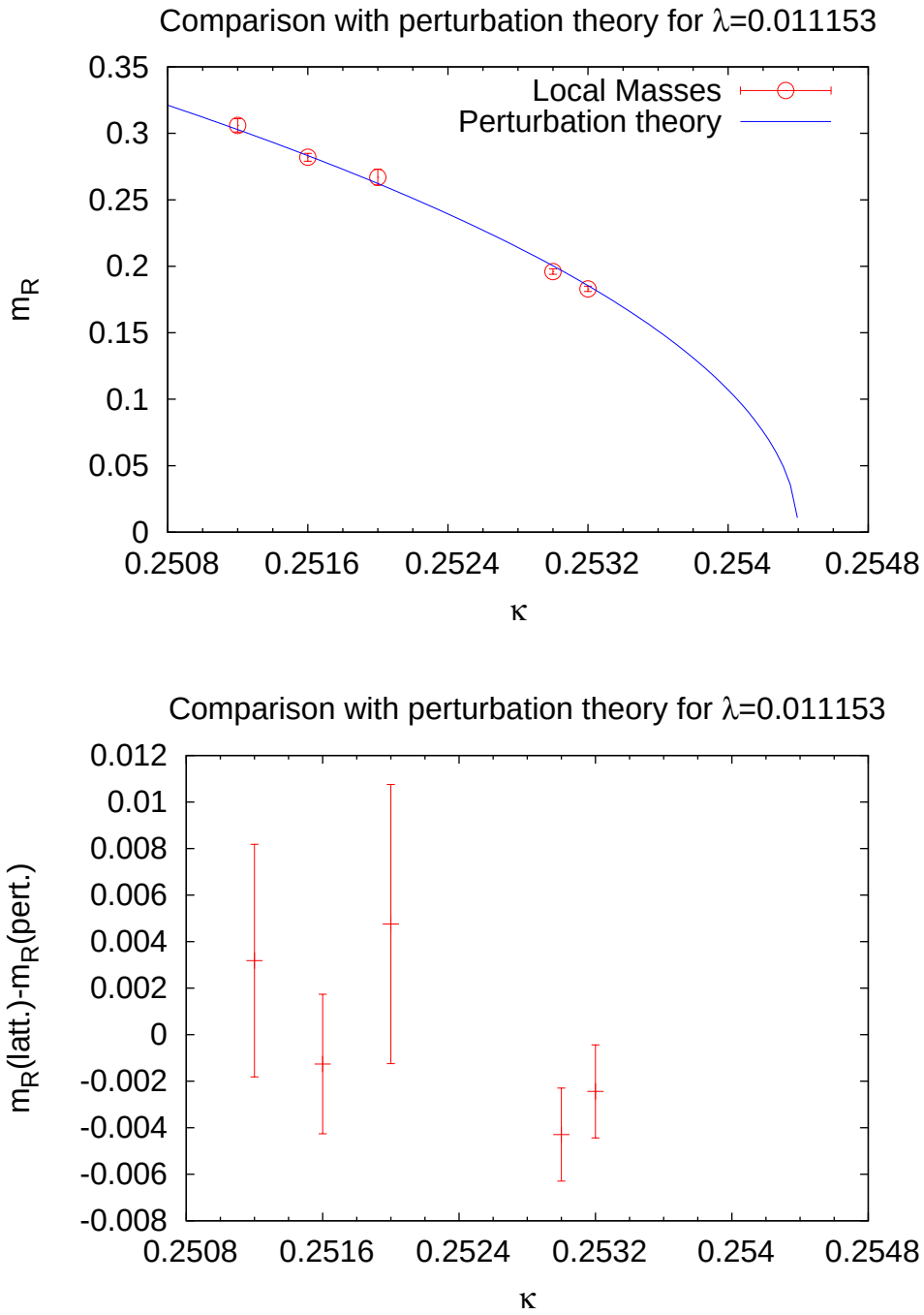

Figure 2: Comparison of extracted local mass with that obtained from RG equations. The integration of the Callan-Symanzik is done using the procedure described in [2].

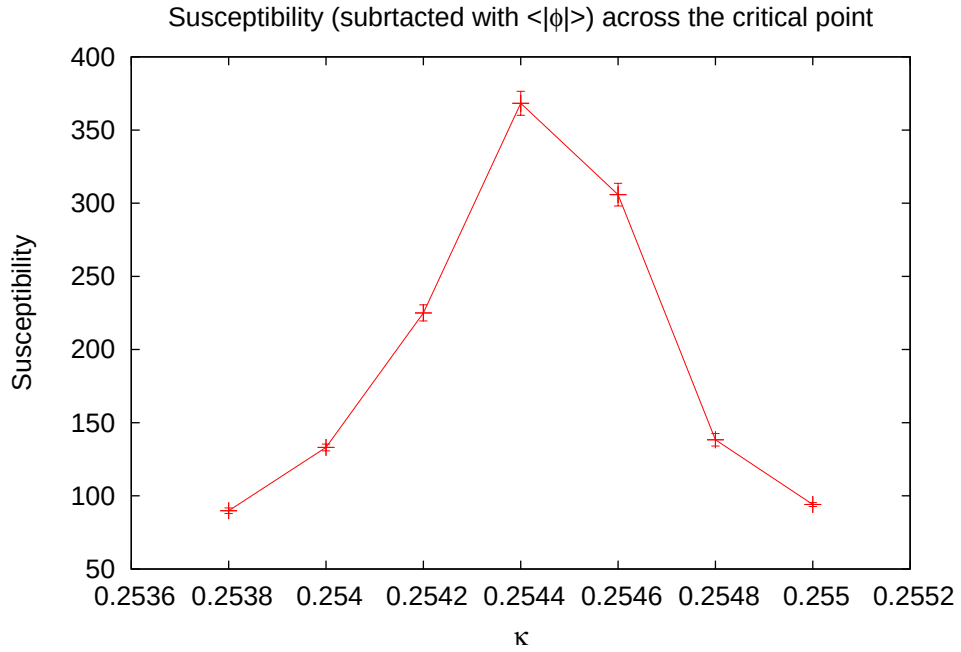

Figure 3: The susceptibility peak to locate the phase transition point. Lattice size:16^4.

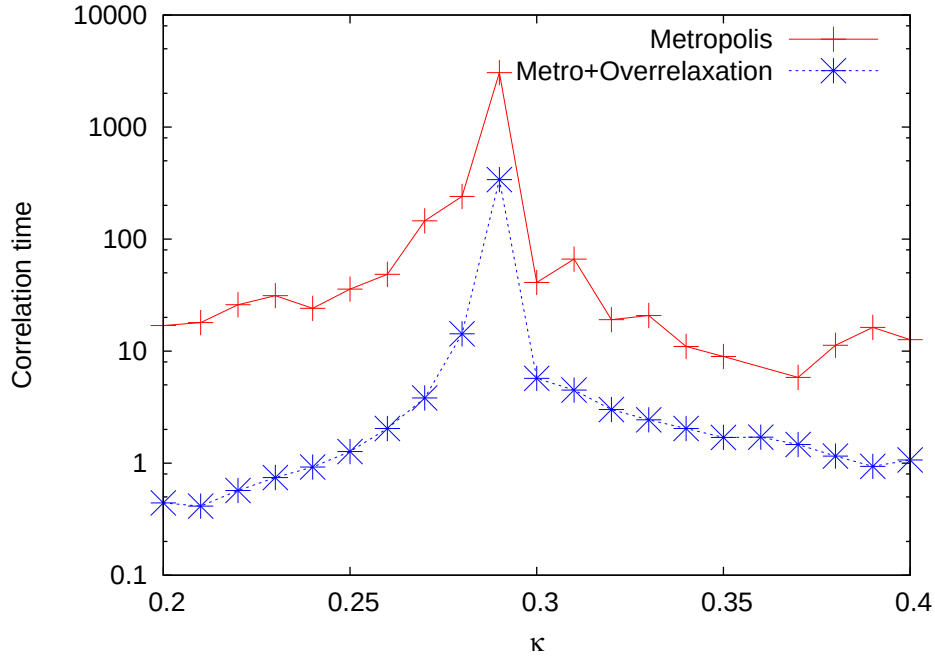

Figure 4: Comparison of the Autocorrelation times in a Metropolis and overrelaxation algorithm

Table 2: Run details of the code

	Metropolis	Overrelaxation improved Metropolis
Spin update times	$\sim 10ns$	$\sim 60ns$
Time to generate indep configs*	$1s$	$0.4s$
compiler	Intel C/C++ compiler	
compiler version	9.1	
compiler flags	-fast	
CPU	Intel Xeon CPU@ 3.0 GHz	

*Configurations that were separated by $3\tau_{int}$ are taken to be independent for this comparison.

3.5 Error Analysis

The variance was calculated by binning the data for different bin sizes. It was checked that for large enough bin size, the Central Limit Theorem is followed and the variance estimates show a plateau. The acceptable bin size would have to be bigger than the minimum bin size above which the calculated variance becomes flat. A typical plot showing the bin-size dependence of the variance for all the measured operators at a particular coupling and boundary condition is shown in fig 5. In all the cases, it was found that the value of the minimum bin size was $\sim$ 1000. We adopted the jackknife analysis [24] [25] [26] in calculating the errors where we took the number of blocks to be 20. The size of our data was such that the size of each bin was $\sim$ 10000 and larger, ensuring that we were well above the minimum bin size limit.

When it was necessary to determine the errors on the masses extracted non perturbatively from the correlators [27], a covariance matrix was constructed to take account of the fact that the measurements are correlated. The covariance matrix was used to estimate the zero temperature masses used as parameters for further calculations of the thermodynamic quantities. The details of this procedure are given in [20].

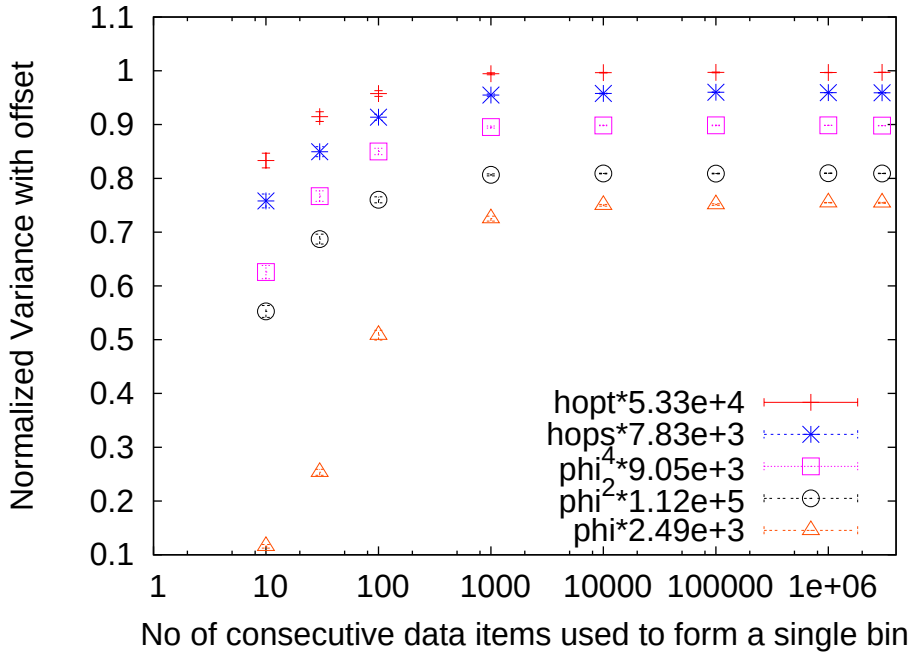

Figure 5: Dependence of the variance on the bin size. Simulation done at couplings: ($\kappa = 0.2516$,$\lambda = 0.011153$) on lattice 20^4 with statistics 9.5×10^6

Chapter 4

Physics Results

4.1 Choice of points for simulation

The simulations were done on lines of constant g_R. On these lines the physics at low energies remain constant and they go by the name of Renormalization Group(RG) trajectories. On a specific RG trajectory a point was chosen where the scaling violations were expected to be negligible. As defined in [2], a "scaling region" is a region in the phase diagram where the low energy amplitudes depend only weakly on the cutoff. The region where one can neglect the scaling violations has been worked out in [2]. In this region a weak-coupling perturbation theory is applicable in the computation of zero-temperature physics. The first simulations were performed at $(\kappa = 0.2516, \lambda = 0.011153)$ taking care that the lattice volume was more than three times the corresponding Compton wavelength. The physical mass was extracted non-perturbatively at this point [20]. To keep the physics constant as we approach the continuum limit, we restrict ourselves to the RG trajectory passing through this point (which we have labelled as A) and try to reach points where the cutoff effects play a lesser role while still having a sufficiently large lattice such that the finite volume effects are under control. Points B, C and D lying on the same RG trajectory were chosen such that the cutoff effects at those points are lesser than

that at point A by factors of 4/5, 2/3 and 1/2 respectively. Finite size scaling is done to establish the thermodynamic limit. That is the major object of the rest of the work. To achieve this the following procedure was adopted:

1. From the values of (κ, λ) and extracted ma, g_R was obtained upto 1-loop order in perturbation theory. For this the following relation was used [21]:

$$g_R = g_0 - \frac{3}{2} g_0^2 J_2(m_R) \tag{33}$$

   where J_2 is the contribution of the diagrams shown in fig 1 that contribute to coupling constant renormalization.

2. Then a smaller mass value was chosen (e.g. that for point B) which we wanted to study. This value was reinserted in eq.(33) and it was solved for g_0, *keeping the value of g_R fixed as obtained in the last step.*

3. Once g_0 is obtained, we can get an estimate of the required (κ, λ) using the eqn 12.

4. A narrow scan in κ was done about the predicted values to ensure that the estimate of the physical mass is indeed correct.

5. As a self consistency check g_R was recalculated at this new point. For all the points considered this way, the variation in g_R was less than 1 percent.

The points for simulation obtained this way are shown in the fig 6 and the parameters at these points are listed in table 3.

Inaccuracies :Clearly, the use of 1 loop in perturbation theory is a crude approximation but was done since the results for the higher loops were not readily available. Physically, this could imply that we might not lie in the "actual" trajectory for all the points and in such a case the continuum limit may not be obtained from the results. However the existence of the thermodynamic limit can still be examined from our results as shown later.

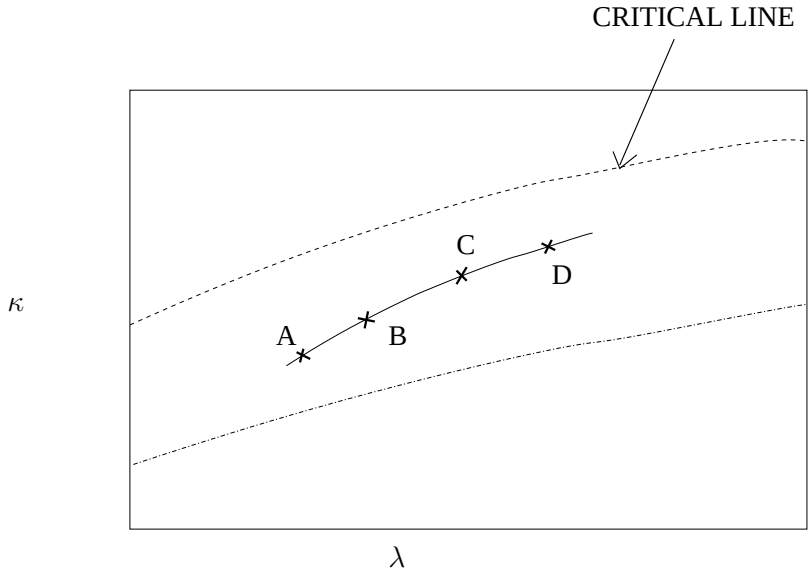

Figure 6: A cartoon showing the relative positions of the points on which the simulations were done. Above the critical line there is the broken phase; while above the lower dashed line and below the critical line is the region where the perturbative Callan-Symanzik equations can be applied [2].

Table 3: Parameter values at each of the different points. g_R is calculated in 1 loop perturbation theory. For comparison, estimate of mass in 1 loop perturbation theory is also shown. For details of the analysis of masses see section 3.5.

No.	κ	λ	g_R	ma	ma(in 1 loop)
A	0.2516	0.011153	3.1772	0.2853 ± 0.0002	0.3012
B	0.2526	0.0117	3.18955	0.2376 ± 0.0003	0.2586
C	0.253452	0.0122	3.16478	0.1897 ± 0.0002	0.2172
D	0.25438	0.0134	3.17108	0.1416 ± 0.0002	0.1834

Table 4: Operator expectation values at point A. For a note on error analysis see section 3.5

LT	$\langle\phi^2\rangle$	$\langle\phi^4\rangle$	$\langle hops\rangle$	$\langle hopt\rangle$
$N_t = 4$				
2	0.61822 ± 0.00005	1.1118 ± 0.0001	0.3821 ± 0.0001	0.13156 ± 0.00004
3	0.61030 ± 0.00002	1.08442 ± 0.00006	0.35707 ± 0.00004	0.12338 ± 0.00002
4	0.60906 ± 0.00001	1.08014 ± 0.00003	0.35316 ± 0.00001	0.12210 ± 0.00001
$N_t = 6$				
2	0.60402 ± 0.00001	1.06286 ± 0.00004	0.34018 ± 0.00003	0.11394 ± 0.00001
3	0.603018 ± 0.000005	1.05945 ± 0.00002	0.33702 ± 0.00001	0.112902 ± 0.000004
4	0.602928 ± 0.000003	1.05914 ± 0.00001	0.336713 ± 0.000006	0.112804 ± 0.000002

Table 5: Operator expectation values at point B. For a note on error analysis see section 3.5

LT	$\langle\phi^2\rangle$	$\langle\phi^4\rangle$	$\langle hops\rangle$	$\langle hopt\rangle$
$N_t = 4$				
2	0.62600 ± 0.00006	1.1374 ± 0.0002	0.4064 ± 0.0002	0.13980 ± 0.00006
3	0.61437 ± 0.00003	1.0970 ± 0.0001	0.36974 ± 0.00009	0.12775 ± 0.00003
4	0.612187 ± 0.000008	1.08948 ± 0.00002	0.36286 ± 0.00002	0.125485 ± 0.000008
$N_t = 6$				
2	0.60719 ± 0.00001	1.07232 ± 0.00004	0.35014 ± 0.00003	0.11730 ± 0.00001
3	0.605310 ± 0.000004	1.06590 ± 0.00002	0.344236 ± 0.000009	0.115359 ± 0.000003
4	0.605095 ± 0.000002	1.065167 ± 0.000008	0.343531 ± 0.000006	0.115127 ± 0.000002

4.2 Measurement of EOS

4.2.1 Operator expectation values

To get the equation of state, first we tabulate the operator expectation values. The errors on these measurements were calculated according to the discussion in section 3.5. The results of these measurements are shown in the tables 4, 5, 6 and 7.

4.2.2 Zero temperature subtraction

Zero temperature subtraction has been discussed in section 2.2. To have an idea of the correct subtraction scheme to be used in our case, we performed subtraction

Table 6: Operator expectation values at point C. For a note on error analysis see section 3.5

LT	$\langle\phi^2\rangle$	$\langle\phi^4\rangle$	$\langle hops\rangle$	$\langle hopt\rangle$
$N_t = 4$				
2	0.63622 ± 0.00006	1.1718 ± 0.0002	0.4385 ± 0.0002	0.15056 ± 0.00006
3	0.61956 ± 0.00002	1.11363 ± 0.00008	0.38603 ± 0.00008	0.13329 ± 0.00003
4	0.61576 ± 0.00001	1.10052 ± 0.00005	0.37408 ± 0.00004	0.12936 ± 0.00001
$N_t = 6$				
2	0.61133 ± 0.00003	1.0852 ± 0.0001	0.3632 ± 0.0001	0.12169 ± 0.00003
3	0.60788 ± 0.00001	1.07343 ± 0.00004	0.35236 ± 0.00003	0.11811 ± 0.00001
4	0.607335 ± 0.000005	1.07156 ± 0.00002	0.35064 ± 0.00001	0.117545 ± 0.000004

Table 7: Operator expectation values at point D. For a note on error analysis see section 3.5

LT	$\langle\phi^2\rangle$	$\langle\phi^4\rangle$	$\langle hops\rangle$	$\langle hopt\rangle$
$N_t = 4$				
2	0.6469 ± 0.0001	1.2055 ± 0.0005	0.4739 ± 0.0004	0.1624 ± 0.0001
3	0.62525 ± 0.00005	1.1300 ± 0.0002	0.4057 ± 0.0002	0.13992 ± 0.00006
4	0.61927 ± 0.00003	1.10939 ± 0.00009	0.38682 ± 0.00009	0.13369 ± 0.00003
$N_t = 6$				
2	0.61647 ± 0.00004	1.0997 ± 0.0001	0.3811 ± 0.0001	0.12769 ± 0.00004
3	0.61030 ± 0.00001	1.07866 ± 0.00005	0.36169 ± 0.00004	0.12126 ± 0.00002
4	0.609051 ± 0.000008	1.07440 ± 0.00003	0.35776 ± 0.00002	0.119956 ± 0.000008

on the operators of a $N_s^3 \times 4$ lattice using the corresponding values obtained using lattices ranging from 40^4 till N_s^4 at point C. The results for the thermodynamic quantities are displayed in figures 7 and 8. Our results indicate that a plateau is reached for all the thermodynamic quantities when the subtraction lattices used N^4 are much greater than N_s^4. In particular, the result of subtracting with a 40^4 lattice agrees with the results obtained by subtraction from the N^4 lattices except when N is comparable to N_s. Thus, we chose to subtract using the largest lattices that we have simulated which is 40^4.

Erratic jumps of the data are observed in the results for the lattices 32^4 and 36^4. We have been unable to account for the jumps. General investigation involving giving reruns at the same couplings with different initial conditions and random number seeds yielded the same results. Moreover reanalyzing the datasets by differing the number of jackknife blocks etc. again produced the same results.

4.2.3 Thermodynamic Quantities

Having determined the subtracted operators, it is straightforward to use the formulae in eqn.(30) to get results for energy density, pressure and the "interaction measure". These results are displayed in tables 8, 9, 10 and 11. The issue that we study here is the thermodynamic limit for which we use finite size scaling.

4.2.4 Finite Size scaling

To establish the thermodynamic limit at constant physics we compare the $N_t = 4$ and the $N_t = 6$ lattices at each of the four different points. The parameters that affect the finite size effects are mL and LT; since these are the only dimensionless quantities that can be constructed that have an explicit volume dependence. To have a quantitative understanding of the finite size effects, we tabulate the local slopes for the thermodynamic quantities as a function of LT (see table 12) and plotted in figures 9, 10 and 11.

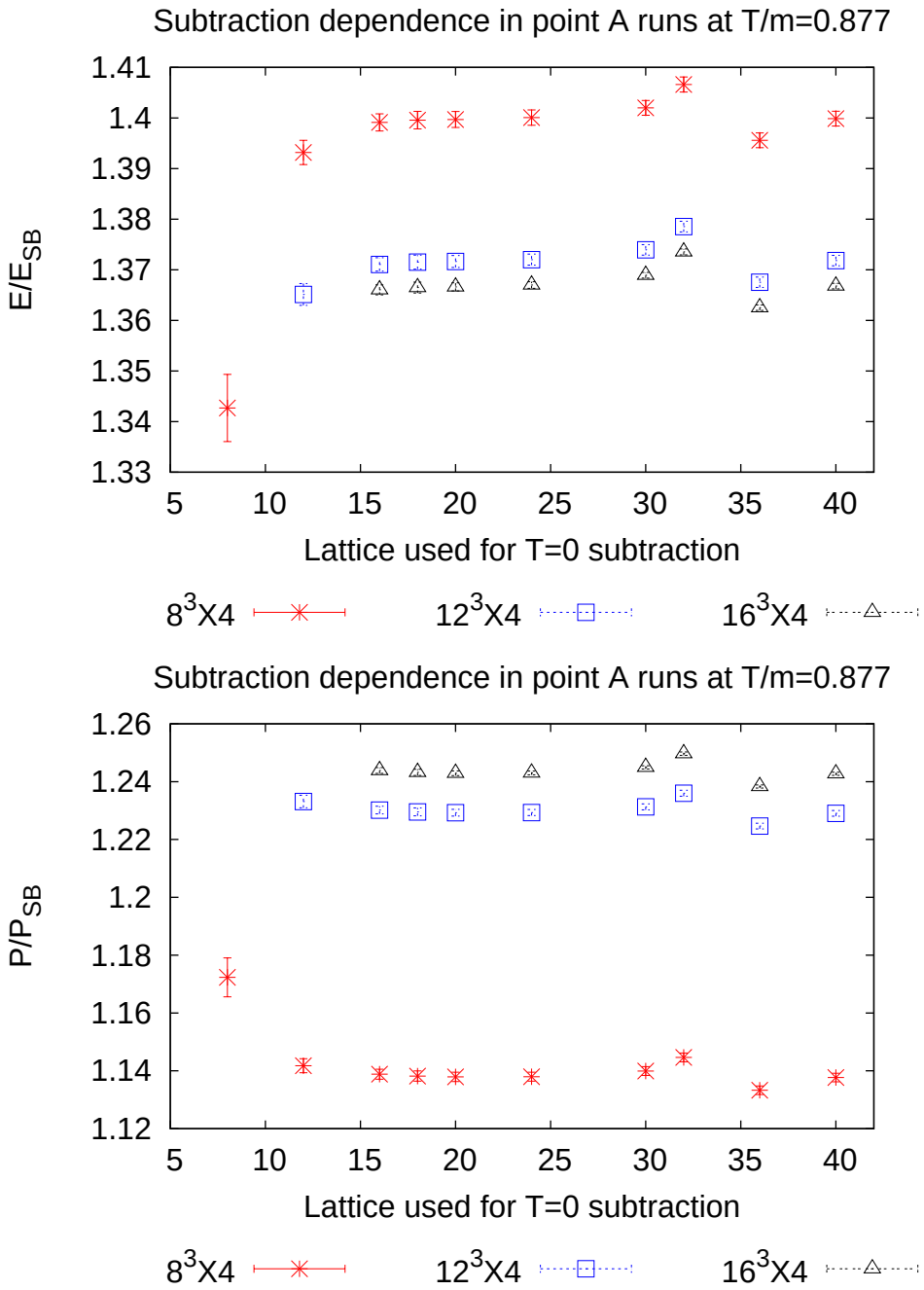

Figure 7: Comparison of different subtraction schemes on the E/E_{SB} and P/P_{SB} at point A

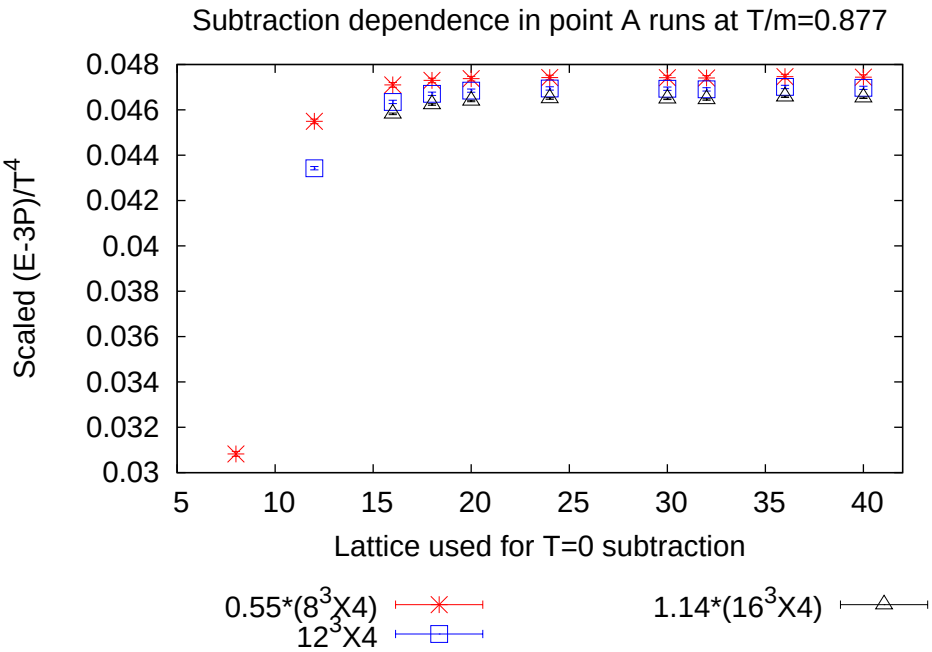

Figure 8: Comparison of different subtraction schemes on the $(E-3P)/T^4$ at point A

Table 8: Thermodynamic quantities at point A in lattice units. For a note on error analysis see section 3.5

LT	E	P	$E-3P$
$N_t=4$			
2	$(1.799 \pm 0.002) \times 10^{-3}$	$(4.873 \pm 0.005) \times 10^{-4}$	$(3.369 \pm 0.007) \times 10^{-4}$
3	$(1.763 \pm 0.001) \times 10^{-3}$	$(5.265 \pm 0.004) \times 10^{-4}$	$(1.835 \pm 0.003) \times 10^{-4}$
4	$(1.7565 \pm 0.0007) \times 10^{-3}$	$(5.323 \pm 0.002) \times 10^{-4}$	$(1.594 \pm 0.001) \times 10^{-4}$
$N_t=6$			
2	$(2.461 \pm 0.007) \times 10^{-4}$	$(6.15 \pm 0.02) \times 10^{-5}$	$(6.16 \pm 0.02) \times 10^{-5}$
3	$(2.392 \pm 0.006) \times 10^{-4}$	$(6.57 \pm 0.02) \times 10^{-5}$	$(4.212 \pm 0.006) \times 10^{-5}$
4	$(2.391 \pm 0.004) \times 10^{-4}$	$(6.63 \pm 0.01) \times 10^{-5}$	$(4.025 \pm 0.004) \times 10^{-5}$

Table 9: Thermodynamic quantities at point B in lattice units. For a note on error analysis see section 3.5

LT	E	P	$E-3P$
$N_t=4$			
2	$(1.948 \pm 0.002) \times 10^{-3}$	$(5.481 \pm 0.007) \times 10^{-4}$	$(3.039 \pm 0.008) \times 10^{-4}$
3	$(1.863 \pm 0.001) \times 10^{-3}$	$(5.698 \pm 0.004) \times 10^{-4}$	$(1.537 \pm 0.004) \times 10^{-4}$
4	$(1.845 \pm 0.001) \times 10^{-3}$	$(5.731 \pm 0.003) \times 10^{-4}$	$(1.255 \pm 0.001) \times 10^{-4}$
$N_t=6$			
2	$(2.86 \pm 0.01) \times 10^{-4}$	$(7.48 \pm 0.04) \times 10^{-5}$	$(6.10 \pm 0.01) \times 10^{-5}$
3	$(2.693 \pm 0.009) \times 10^{-4}$	$(7.75 \pm 0.03) \times 10^{-5}$	$(3.670 \pm 0.004) \times 10^{-5}$
4	$(2.677 \pm 0.009) \times 10^{-4}$	$(7.80 \pm 0.03) \times 10^{-5}$	$(3.379 \pm 0.003) \times 10^{-5}$

Table 10: Thermodynamic quantities at point C in lattice units. For a note on error analysis see section 3.5

LT	E	P	$E-3P$
$N_t=4$			
2	$(2.146 \pm 0.002) \times 10^{-3}$	$(6.336 \pm 0.005) \times 10^{-4}$	$(2.457 \pm 0.005) \times 10^{-4}$
3	$(1.982 \pm 0.001) \times 10^{-3}$	$(6.210 \pm 0.003) \times 10^{-4}$	$(1.190 \pm 0.002) \times 10^{-4}$
4	$(1.9450 \pm 0.0007) \times 10^{-3}$	$(6.183 \pm 0.002) \times 10^{-4}$	$(9.002 \pm 0.008) \times 10^{-5}$
$N_t=6$			
2	$(3.446 \pm 0.009) \times 10^{-4}$	$(9.61 \pm 0.03) \times 10^{-5}$	$(5.61 \pm 0.02) \times 10^{-5}$
3	$(3.063 \pm 0.007) \times 10^{-4}$	$(9.22 \pm 0.02) \times 10^{-5}$	$(2.981 \pm 0.007) \times 10^{-5}$
4	$(3.011 \pm 0.006) \times 10^{-4}$	$(9.18 \pm 0.02) \times 10^{-5}$	$(2.563 \pm 0.003) \times 10^{-5}$

Table 11: Thermodynamic quantities at point D in lattice units. For a note on error analysis see section 3.5

LT	E	P	$E-3P$
$N_t=4$			
2	$(2.476 \pm 0.004) \times 10^{-3}$	$(7.76 \pm 0.01) \times 10^{-4}$	$(1.465 \pm 0.005) \times 10^{-4}$
3	$(2.168 \pm 0.002) \times 10^{-3}$	$(6.989 \pm 0.006) \times 10^{-4}$	$(7.18 \pm 0.02) \times 10^{-5}$
4	$(2.082 \pm 0.002) \times 10^{-3}$	$(6.770 \pm 0.005) \times 10^{-4}$	$(5.10 \pm 0.01) \times 10^{-5}$
$N_t=6$			
2	$(4.66 \pm 0.02) \times 10^{-4}$	$(1.415 \pm 0.006) \times 10^{-4}$	$(4.13 \pm 0.01) \times 10^{-5}$
3	$(3.68 \pm 0.01) \times 10^{-4}$	$(1.161 \pm 0.004) \times 10^{-4}$	$(1.973 \pm 0.005) \times 10^{-5}$
4	$(3.48 \pm 0.01) \times 10^{-4}$	$(1.109 \pm 0.004) \times 10^{-4}$	$(1.536 \pm 0.003) \times 10^{-5}$

The results show that as we decrease ma at fixed LT the finite size effects become larger, as expected. It is also seen that at fixed m and for the same N_t, the absolute value of the slope decreases with larger LT. In particular, for the $N_t = 6$ lattices, for energy density and pressure, the local slope between the $LT = 3$ and $LT = 4$ is zero within error. The $N_t = 4$ and $N_t = 6$ lattices at fixed m can be compared by looking at the slopes of the thermodynamic quantities as a function of LT. The local slope for $N_t = 6$ would be lesser than the $N_t = 4$ counterparts for the same range of LT. This comparison also yields the expected results except in the case of the smallest mass.

From the results, we can definitely conclude that the thermodynamic limit is reached for the $LT = 4$ runs for the masses $ma = 0.2853$ and $ma = 0.2376$ since the numerical values of the slopes between $LT = 3$ and $LT = 4$ are zero within error. For the last two points where the finite size effects are large the situation is less clear.

Table 12: Local slopes for thermodynamic quantities

	$LT = 2\&3$		$LT = 3\&4$	
ma	$N_t = 4$	$N_t = 6$	$N_t = 4$	$N_t = 6$
Slopes for E/T^4				
0.2853	$(9.2 \pm 0.6) \times 10^{-3}$	$(9 \pm 1) \times 10^{-3}$	$(1.6 \pm 0.4) \times 10^{-4}$	$(2 \pm 9) \times 10^{-4}$
0.2376	$(2.17 \pm 0.06) \times 10^{-2}$	$(2.1 \pm 0.2) \times 10^{-2}$	$(4.7 \pm 0.4) \times 10^{-3}$	$(2 \pm 2) \times 10^{-3}$
0.1897	$(4.21 \pm 0.05) \times 10^{-2}$	$(4.9 \pm 0.2) \times 10^{-2}$	$(9.5 \pm 0.3) \times 10^{-3}$	$(7 \pm 1) \times 10^{-3}$
0.1416	$(7.9 \pm 0.1) \times 10^{-2}$	$(1.27 \pm 0.03) \times 10^{-1}$	$(2.22 \pm 0.06) \times 10^{-2}$	$(2.6 \pm 0.2) \times 10^{-2}$
Slopes for P/T^4				
0.2853	$(-1.00 \pm 0.02) \times 10^{-2}$	$(-5.4 \times 0.4) \times 10^{-3}$	$(-1.5 \pm 0.1) \times 10^{-3}$	$(-7 \pm 3) \times 10^{-4}$
0.2376	$(-5.5 \pm 0.2) \times 10^{-3}$	$(-3.5 \pm 0.7) \times 10^{-3}$	$(-8 \pm 1) \times 10^{-4}$	$(-6 \pm 6) \times 10^{-4}$
0.1897	$(3.2 \pm 0.2) \times 10^{-3}$	$(5.1 \pm 0.5) \pm 10^{-3}$	$(7 \pm 1) \times 10^{-4}$	$(5 \pm 4) \times 10^{-4}$
0.1416	$(1.99 \pm 0.03) \times 10^{-2}$	$(3.29 \pm 0.09) \times 10^{-2}$	$(5.6 \pm 0.2) \times 10^{-3}$	$(6.7 \pm 0.8) \times 10^{-3}$
Slopes for $(E - 3P)/T^4$				
0.2853	$(3.92 \pm 0.02) \times 10^{-2}$	$(2.52 \pm 0.03) \times 10^{-2}$	$(6.15 \pm 0.08) \times 10^{-3}$	$(2.42 \pm 0.09) \times 10^{-3}$
0.2376	$(3.84 \pm 0.02) \times 10^{-2}$	$(3.14 \pm 0.02) \times 10^{-2}$	$(7.22 \pm 0.09) \times 10^{-3}$	$(3.78 \pm 0.07) \times 10^{-3}$
0.1897	$(3.24 \pm 0.01) \times 10^{-2}$	$(3.41 \pm 0.03) \times 10^{-2}$	$(7.42 \pm 0.05) \times 10^{-3}$	$(5.4 \pm 0.1) \times 10^{-3}$
0.1416	$(1.91 \pm 0.01) \times 10^{-2}$	$(2.80 \pm 0.02) \times 10^{-2}$	$(5.33 \pm 0.05) \times 10^{-3}$	$(5.66 \pm 0.08) \times 10^{-3}$

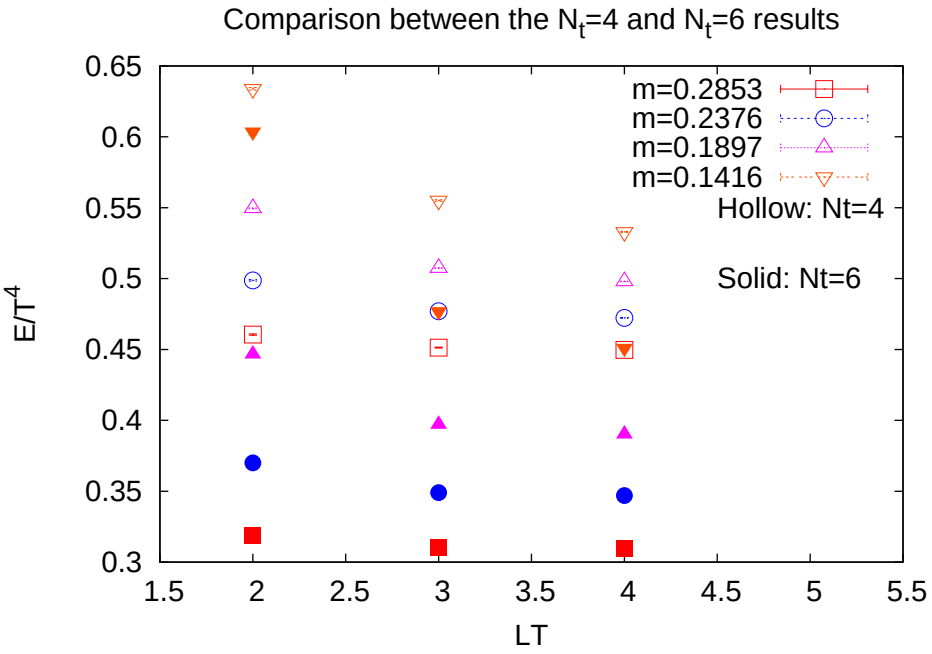

Figure 9: Scaling of the E/T^4 for $N_t = 4$ and $N_t = 6$.

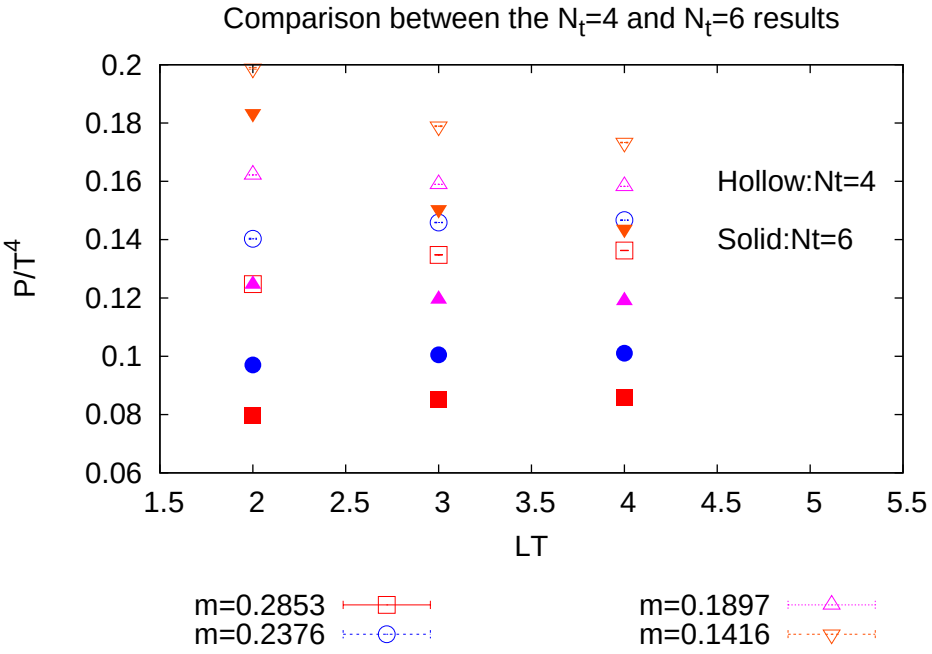

Figure 10: Scaling of the P/T^4 for $N_t = 4$ and $N_t = 6$.

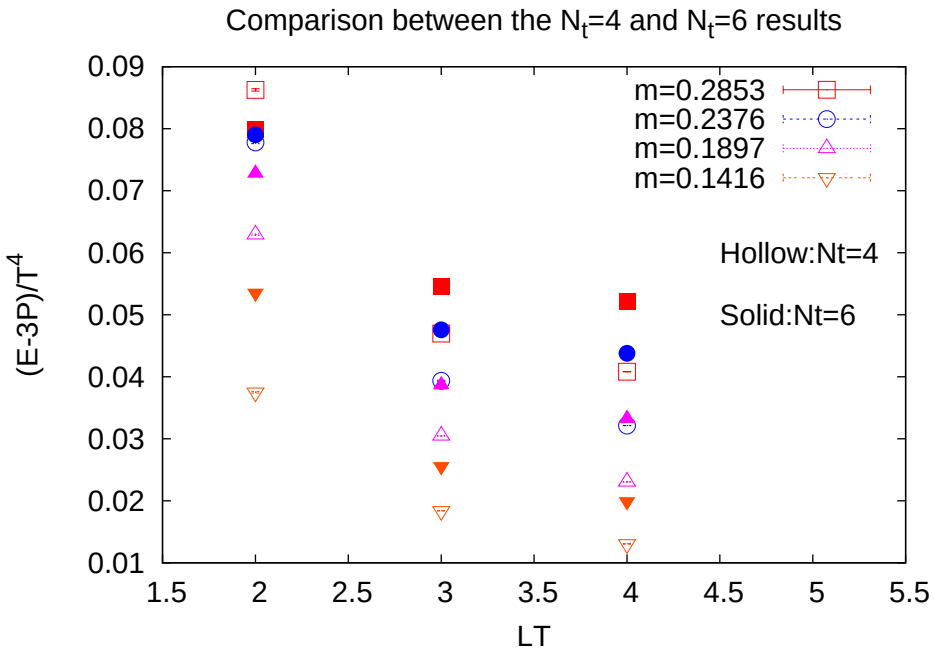

Figure 11: Scaling of $(E-3P)/T^4$ for $N_t = 4$ and $N_t = 6$.

Chapter 5

Conclusion

In this work we have studied the thermodynamics of an interacting ϕ^4 theory in 4 space-time dimensions with the action given in equation 10. We have used perturbation theory to 1 loop order to evaluate the β and γ functions (eqn. 22) and the anisotropy coefficients (eqn. 25,26). In particular this is the first report for the calculation of the anisotropy coefficient upto 1 loop in an interacting ϕ^4 theory. The renormalisation conditions used are stated in section 2.2.1. The expressions used for the thermodynamic quantities are listed in section 2.3.

The algorithms used in the numerical study are explained in the sections 3.1 and 3.2. The numerical checks that were made with existing results in the literature are tabulated in table 1. The technical specifications of the machines used to run the code and estimate of the run times are covered in table 2. A note on error analysis is given in section 3.5.

The choice of the points for simulation are discussed in section 4.1. The results of the measurements of the operators and the thermodynamic quantities in lattice units are given in tables 4 to 11. Removal of ultraviolet divergences via subtraction is the subject of section 4.2.2. A discussion on the thermodynamic limit is given in section 4.2.4.

Future work will consider smaller lattice spacings keeping the physical parameters constant and thus taking the continuum limit.

Bibliography

[1] K. G. Wilson and J Kogut. The renormalisation group and the ϵ expansion. *Physics Reports*, 12C, 75, 1974.

[2] M Lüscher and P Weisz. Scaling laws and triviality bounds in the lattice ϕ^4 theory,i. one-component model in the symmetric phase. *Nucl. Physics*, B 290, 25, 1988.

[3] M Lüscher and P Weisz. Scaling laws and triviality bounds in the lattice ϕ^4 theory,ii. one-component model in the phase with spontaneous symmetry breaking. *Nucl. Physics*, B 295, 65, 1988.

[4] J Balog et al. The 4d one component lattice ϕ^4 model in the broken phase revisited. *Nucl. Physics*, B 714, 256, 2005.

[5] M Lüscher. Volume dependence of the energy spectrum in massive quantum field theories,i stable particle states. *Comm. Math. Phy.*, 104, 177, 1986.

[6] M Lüscher. Volume dependence of the energy spectrum in massive quantum field theories,ii scattering states. *Comm. Math. Phy.*, 105, 153, 1986.

[7] I Montvay. Numerical study of finite volume effects in the 4d ising model. *Nucl. Physics*, B 290, 327, 1987.

[8] R Brower and P Tamayo. Embedded dynamics for ϕ^4 theory. *Phys. Rev. Lett.*, 62, 10, 1989.

[9] C Morningstar. The monte carlo method in quantum field theory. *Lectures given at the 21st annual Hampton University Graduate Studies (HUGS) Program at Jefferson Lab, arXiv:hep-lat/0702020*, 2007.

[10] M Creutz. Monte carlo study of quantized su(2) gauge theory. *Phys. Rev. D*, 21, 8, 1980.

[11] J Engels et al. Gauge field thermodynamics for the su(2) yang-mills system. *Nucl. Phy.*, B 205, 547, 1982.

[12] F Karsch. Su(n) gauge theory couplings on asymetric lattices. *Nucl. Phy.*, B 205, 285, 1982.

[13] J Engels et al. Finite size effects in euclidean lattice thermodynamics for non-interacting bose and fermi systems. *Nucl. Phy.*, B 205, 239, 1982.

[14] M Gorenstein et al. Thermodynamics of massive bose field on a lattice: Finite size effects and glueball mass estimate. *J. Phys. G*, 11, 143, 1985.

[15] M Gorenstein et al. Zero mode effects in the lattice thermodynamics of massless bose field. *ITF-85-15-E*, 1985.

[16] R M Ricotta. Thermodynamics of free massless bose field on a lattice. *IMPERIAL/TP/85-86/23*, 1986.

[17] H Li and T Chen. Analytical study of finite temperature lattice ϕ^4 theory. *Phys. Lett B*, 347, 131, 1995.

[18] H Li and T Chen. Phase structure and critical behavior of lattice phi**4 theory at different temperatures. *Z.Phys.C*, 74, 151, 1997.

[19] N Metropolis et al. Equations of state calculation by fast computing machines. *J. Chem. Phys.*, 21, 1087,1953.

[20] Banerjee D. Mass extraction in lattice field theories. *Project Report*, TIFR, 2008.

[21] Montvay I and Müenster G. Quantum fields on the lattice. *Cambridge Monographs in Physics*, Chapter 2, 1994.

[22] Press et al. Numerical recipes in c. *Cambridge University Press*, 1992.

[23] S Wolfram et al. Mathematica 5.2.

[24] Efron B. Computers and the theory of statistics: Thinking the unthinkable. *SIAM Review*, 21, 4, 1979.

[25] A Billoire et al. Dynamics near a first order phase transition with the metropolis and swedsen-wang algorithms. *Nucl. Phys.*, B, 358, 231, 1991.

[26] S Gottlieb et al. Hadronic coupling constants in lattice gauge theory. *Nucl. Phys.*, B, 263, 704, 1986.

[27] Parisi G. The strategy for computing the hadronic mass spectrum. *Phys. Rept.*, 103, 203, 1984.